

## Article

# The Secreted Metabolome of Hela Cells under Effect of Crostamine, a Cell-Penetrating Peptide from a Rattlesnake Using NMR-Based Metabolomics Analyses

Mônika Aparecida Coronado <sup>1,\*</sup>, Fábio Rogério de Moraes <sup>2,†</sup>, Bruna Stuqui <sup>3,4,†</sup>, Marília Freitas Calmon <sup>3</sup>, Raphael Josef Eberle <sup>1,5</sup>, Paula Rahal <sup>3</sup> and Raghuvir Krishnaswamy Arni <sup>2,\*</sup>

- <sup>1</sup> Institute of Biological Information Processing (IBI-7: Structural Biochemistry), Forschungszentrum Jülich, 52428 Jülich, Germany; r.eberle@fz-juelich.de
- <sup>2</sup> Multiuser Center for Biomolecular Innovation, Department of Physics, São Paulo State University (UNESP), São José do Rio Preto 15054-000, Brazil; fabiom@sjrp.unesp.br
- <sup>3</sup> Laboratory of Genomic Studies, Department of Biology, São Paulo State University (UNESP), São José do Rio Preto 15054-000, Brazil; bru.stuqui@gmail.com (B.S.); macal131@gmail.com (M.F.C.); p.rahal@unesp.br (P.R.)
- <sup>4</sup> Instituto Federal de Educação, Ciência e Tecnologia de São Paulo (IFSP), São Paulo 01151-000, Brazil
- <sup>5</sup> Institut für Physikalische Biologie, Heinrich-Heine-Universität Düsseldorf, Universitätsstraße, 40225 Düsseldorf, Germany
- \* Correspondence: m.coronado@fz-juelich.de (M.A.C.); raghuvir.arni@unesp.br (R.K.A.); Tel.: +49-2461-61-9505 (M.A.C.); +55-017-3221-2460 (R.K.A.)
- † These authors contributed equally to this work.



**Citation:** Coronado, M.A.; de Moraes, F.R.; Stuqui, B.; Calmon, M.F.; Eberle, R.J.; Rahal, P.; Arni, R.K. The Secreted Metabolome of Hela Cells under Effect of Crostamine, a Cell-Penetrating Peptide from a Rattlesnake Using NMR-Based Metabolomics Analyses. *BioMed* **2022**, *2*, 238–254. <https://doi.org/10.3390/biomed2020020>

Academic Editor: Wolfgang Graier

Received: 25 January 2022

Accepted: 20 April 2022

Published: 22 April 2022

**Publisher's Note:** MDPI stays neutral with regard to jurisdictional claims in published maps and institutional affiliations.



**Copyright:** © 2022 by the authors. Licensee MDPI, Basel, Switzerland. This article is an open access article distributed under the terms and conditions of the Creative Commons Attribution (CC BY) license (<https://creativecommons.org/licenses/by/4.0/>).

**Abstract:** Sequestering and reprogramming of cellular metabolism represents one of the principal hallmarks of several cells. Antimicrobial peptides have been shown to exhibit selective anticancer activities. In this study, the secreted metabolome of HeLa cells under action of the antimicrobial peptide Crostamine from the venom of the South American rattlesnake *Crotalus durissus terrificus* was evaluated. Crostamine has been shown to be selective for highly proliferating cells and is able to extend the in vivo lifespan. The present study using a cell line of cervical cancer, HeLa cells, provide insights into how Crostamine acts in cell metabolism. NMR spectroscopy was used to identify and quantify relative metabolite levels, which are associated with Crostamine uptake. Statistical analysis reveals that Crostamine dramatically affects metabolites related to glycolysis, metabolism and biosynthesis of amino acids and pyruvate metabolism. The developed machine learning model is found to be robust by ROC curve analysis, suggesting that the metabolic state of HeLa cells treated with Crostamine is different from the control samples. To account for metabolite levels, it is suggested that Crostamine would have to act on glycolysis, which, in turn, affects several other metabolic pathways, such as, glutathione metabolism, TCA cycle and pyruvate metabolism. The observed metabolic changes shed light into the mode of Crostamine function.

**Keywords:** cell-penetrating peptide; Crostamine; anticancer; metabolomics

## 1. Introduction

Diverse factors such as the exposure to carcinogens, viruses, ionizing radiation, chemicals and genetic disorders including cell line mutations trigger the onset of cancer [1]. The Global Burden of Disease (GBD) estimated in 2015, that there were 17.5 million cancer cases worldwide and for 2018 it was estimated to result in 9.6 million deaths. The statistics indicate that the incidence of cancer increased by about 33% between 2005 and 2015 [2].

More than 40 years ago, Human Papillomavirus (HPV) was implicated in causing different human neoplastic lesions [3] and currently, 200 HPV types including cutaneous and mucosal HPV types have been characterized. Cervical cancer (CC) is certainly the most common cancer among women causing significant morbidity and mortality worldwide [4–9].

At the global level, one in 68 women develops CC in their lifetime, the occurrence is higher in developing countries, with 1 in 24 women presenting CC symptoms, and is significantly lower in highly developed countries, where 1 in 115 women developed CC during their lifetimes [2].

According to the National Cancer Institute of Brazil (INCA), the number of new cases of CC for each year of the biennium 2018–2019 was estimated to be 16,370 cases per 100,000 women in Brazil. It represents the seventh recurrent neoplasm in the global female population, and the fourth principal cause of women's mortality by cancer in Brazil [10].

Proteins, peptides and enzymes from animals of different species are being tested for application in cancer therapies and many active secretions produced by animals have been employed in the development of new drugs to treat diseases such as hypertension and cancer. Snake venom toxins have contributed significantly to the treatment of many medical conditions [11] and a host of studies cite the anti-cancer potential of snake venoms [12,13].

Since treatment of cancer is a major challenge and many of the currently used therapies are prohibitively expensive and often trigger undesirable secondary reactions, and since molecules isolated from snake venoms have demonstrated that they retard and inhibit the growth of cancerous cells, they have been the focus of research [12]. Crotamine, extracted from the venom of the Brazilian rattlesnake, *Crotalus durissus terrificus*, is a highly basic (pI 10.3), low molecular weight (42 kDa), non-enzymatic and, non-cytolytic cell-penetrating peptide (CPP) [14–16] that is able to cross the cellular lipid barrier [17–19]. It also exhibits other activities such as: antimicrobial activity [20,21], selectivity for highly proliferating cells [20,22]; inhibits tumor growth [23], and it is also potentially interesting as an individual therapeutic agent since it possesses the ability to transport proteins, peptides, nucleic acids and, perhaps, even entire genes across the cellular membrane [17,24–28].

Selective cytotoxicity of Crotramine in tumor cells has been reported: experiments using Crotramine as an inhibitor resulted in a significant decrease of tumor growth and, mice with tumors showed increased survival rates [23,29] and it has also been demonstrated to possess anti-tumoral activity in cell cultures and animal models [22,23,29,30]. Experiments using in vitro models are more feasible and practical to assess the potential effect of molecules and to understand the underlying mechanisms of physiological processes.

Understanding the cellular responses of Crotramine may provide metabolic information on the reactions of biological systems at the molecular level. The biological interactions in cellular pathways can be elucidated based on the analysis of cell lines using NMR-based metabolomics footprinting assays, to screen promising drugs, and is effective in in vitro screening for identifying significant metabolite changes in response to the administration of diverse molecules [31–33].

In the present study, we utilized an integrated metabolomics approach to systematically investigate the response of Human cervical adenocarcinoma cells (HeLa cell line) using Crotramine as the mediator. Based on the analysis of the metabolic pathway, we identified changes of the cell line pattern. <sup>1</sup>H NMR spectroscopy coupled with pattern recognition and biochemical network analysis was used to characterize the metabolic footprint profile of HeLa cells.

## 2. Materials and Methods

### 2.1. Cell Line

Human cervical adenocarcinoma cell line–HeLa (ATCC CRM-CCL-2) was kindly provided by Luisa Lina Villa (Department of Radiology, Center on Translational Oncology Investigation, São Paulo State Cancer Institute, São Paulo University, Brazil). Cell lines were cultured in Dulbecco's modified Eagle medium (DMEM) (Gibco Life Technologies, Grand Island, NY, USA) supplemented with 10% heat-inactivated fetal bovine serum (FBS), penicillin (50 U/mL), and streptomycin (0.05 mg/mL). Cells were incubated at 37 °C with 5% CO<sub>2</sub>.

## 2.2. MTT Assay

Colorimetric MTT assay was used to evaluate the cytotoxicity in 96-well plates and the medium containing Crotonamine at concentrations of 6, 8, 10, 12, 14, 16, and 20  $\mu\text{M}$  was added to each well containing  $1 \times 10^4$  cells. After 4, 12, and 24 h of incubation with Crotonamine, 100  $\mu\text{L}$  of medium containing 3-(4,5-dimethylthiazol-2-yl)-2,5-diphenyl tetrazolium bromide (MTT) (1 mg/mL) (Merck, Darmstadt, Germany) was added to each well. After 30 min of incubation, the medium was removed, and the formazan crystals were solubilized by incubation for 10 min in 100  $\mu\text{L}$  of DMSO (Sigma-Aldrich). Absorbance of each well was determined at 570 nm. Each experiment was performed in triplicate and in three independent assays.

## 2.3. Crotonamine Treatment and Metabolite Extraction

For cell seeding, HeLa cells were cultured in serum-starved medium. After 24 h, Crotonamine was added to the supplemented culture medium (containing 10% FBS and antibiotics) at concentrations of 10  $\mu\text{M}$ . Crotonamine treatment concentration was chosen based on the results of the MTT assay. To avoid contamination in the cell culture, filter sterilization (using a Millipore filter with a pore size of 0.22  $\mu\text{m}$ ) of the medium containing Crotonamine was applied before introducing the medium to the cell culture. After 24 h of Crotonamine incubation, the medium was submitted to footprint metabolomics studies. The control group received only serum-starved medium by 24 h.

## 2.4. Nuclear Magnetic Resonance Spectroscopy

NMR measurements from sample cultures were performed utilizing a Bruker AVANCE III HD (Bruker Biospin, Ettlingen, Germany), operating at 600 MHz for  $^1\text{H}$  equipped with a triple resonance cryoprobe. The standard NOESYPR1D pulse sequence was used with a recycle delay of 2 s, a mixing time of 100 ms, 16 scans (four dummy scans), collected in 32 k complex data points and a spectral width of 20 ppm. Each free induction decay measurement (FIDs) was multiplied by an exponential function with 1 Hz line-broadening, followed by Fourier transformation in the Bruker TopSpin 3.2.5 (Bruker Biospin, Ettlingen, Germany). Reference in each spectrum was performed internally by setting the lactate methyl doublet at 1.31 ppm. Finally, the residual water region (4.5–5.0 ppm) was deleted from the dataset.

Furthermore, specific regions were previously identified to integral calculation, after metabolite identification. For assisting metabolite identification, selected samples were investigated by  $^1\text{H}$ ,  $^{13}\text{C}$  Heteronuclear Single Quantum Coherence (HSQC) NMR spectroscopy.

## 2.5. Statistical Analysis

Data was organized following MetaboAnalyst guidelines [34] and its web server was used for analysis. First, data was Pareto scaled (mean centered and divided by the square root of the standard deviation), and subsequently, Principal Component Analysis (PCA), Partial Least Square Discriminant Analysis (PLS-DA) and its orthogonal version (OPLS-DA) were performed. First, the complete spectra (excluding the solvent region) were uploaded for evaluating control and treated metabolic differences by means of PCA, PLS-DA and OPLS-DA score plots. Significant signals related to high absolute loadings were subject to metabolite identification. Specific metabolite signals quantified by their integrals were reorganized and uploaded to MetaboAnalyst for further analysis. Univariate *t*-test and fold change analysis were used to compare relative metabolite levels between control and Crotonamine treated HeLa cells. Boxplots and *t*-test p-values were used to check differences in metabolite levels. In addition, PCA, PLS-DA and OPLS-DA were repeated with this reduced dataset to confirm if the used metabolites were able to keep the degree of difference between control and Crotonamine-treated cell lines. Furthermore, machine learning classification methods, Random Forest and Support Vector Machine (SVM) were used to check if the developed models were successful in predicting whether cells were from a control or Crotonamine-treated sample.

To assess the robustness of the developed model with respect to metabolite levels following Crotonamine treatment, Receiver Operating Characteristic (ROC) curves for three different classification algorithms, as available in MetaboAnalyst at Biomarker Analysis module were used. For each model, the web-server uses a Monte-Carlo cross validation scheme where 66% of the data is used to assess feature importance and build the model itself, whereas the remaining 33% are used for validation and performance measurement. This process is then repeated using different metabolites sets. Metabolite importance is assessed according to the frequency of occurrence of a particular metabolite and is selected to compose a classification model.

## 2.6. Metabolite Identification

Metabolites were manually identified using Chemomx profiler (version 8.1, Chemomx Inc., Edmonton, Canada) by matching resonances of random spectra. Cross-peaks were identified in the TOCSY spectra as well as signals from the  $^1\text{H}$ ,  $^{13}\text{C}$ -HSQC. Expected TOCSY and HSQC signals were retrieved from the Human Metabolome Data Bank [35].

## 2.7. Pathway Analysis

Genome-scale metabolic models have been used for gaining insights into the response of metabolic pathways of a variety of different stimuli in context to an organism, a key concept in the system biology approach [36]. The HeLa cell lines metabolic model was generated by using RNA-seq data and evaluated with metabolome mapping, showing interesting results for the identification of cancer related metabolites in different cell lines [37]. In this study, HeLa cells metabolic models were uploaded into MetExplore web server [38] and the observed metabolite levels were used to get insights into the metabolic pathways that were changed by the uptake of Crotonamine.

## 3. Results

### 3.1. Viability of HeLa Cells in Response to the Exposure of Crotonamine

Crotonamine was purified following the procedure of Coronado et al. (2013) [16] and used for cell viability assays. Experimental control cells retained their viability at all analyzed incubation times. After 4, 12 and 24 h of incubation with all the tested concentrations of Crotonamine, HeLa cells demonstrated viabilities greater than 70% (Figure 1). Viability of HeLa cells decreased with increasing Crotonamine concentration; however, the concentrations used in this work demonstrated low cytotoxicity. From these results, the 10  $\mu\text{M}$  concentration and 24 h incubation were chosen, as the results showed significant cell viability of around 90%.

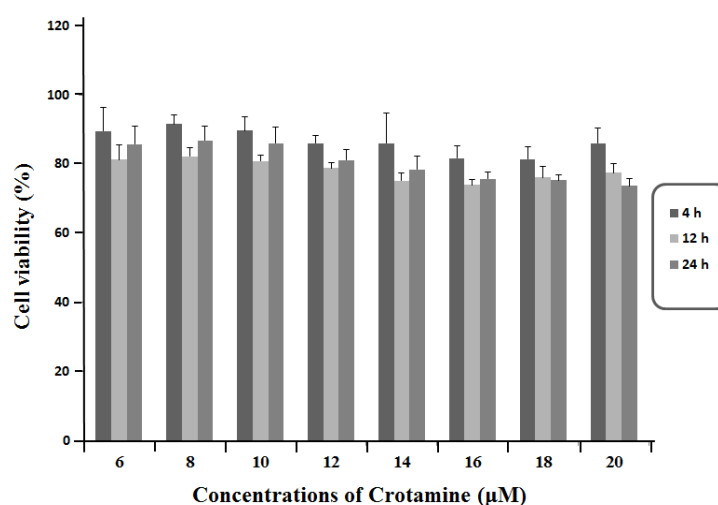


**Figure 1.** Analysis of the cellular effects of Crotonamine on HeLa cells viability. Cell viability assay investigated after 4, 12 and 24 h of incubation with Crotonamine at concentrations of 6, 8, 10, 12, 14, 16, and 20  $\mu\text{M}$ .

### 3.2. Secreted Metabolic Profile of HeLa Cells

We decided to evaluate the secreted metabolomic profiling on HeLa cells treated with 10  $\mu$ M Crotamine after 24h and to compare this with the results for untreated cells.

For the present study, metabolic foot printing has been used to characterize the metabolic changes of HeLa cells subjected to Crotamine. Intensities from NMR spectra were examined, and spectral bins were manually selected to exclude noisy and solvent regions.

Following the treatment of the Crotamine NMR profile of HeLa cells, the observed metabolic differences between control and treated cells (Figure 2-asterisk), indicated that Crotamine induced alterations in the metabolism of HeLa cells.

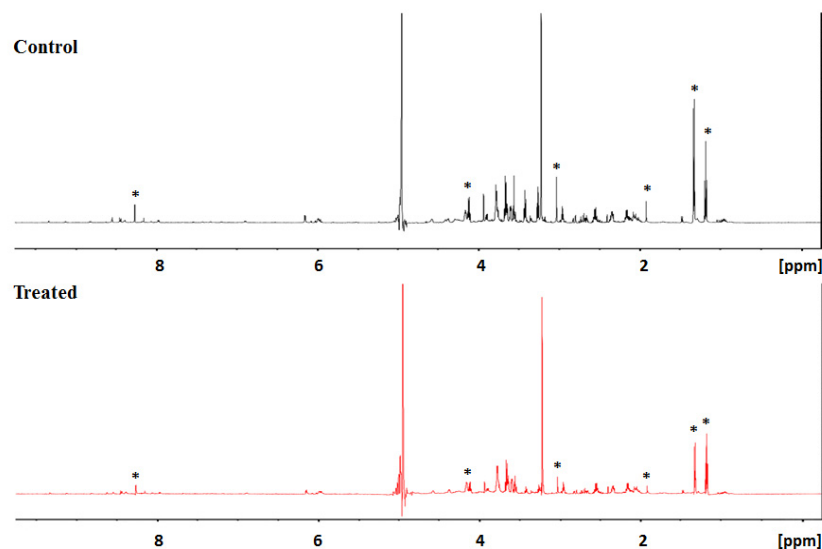


**Figure 2.** NMR spectrum comparison between control and treated HeLa cell sample. Asterisks show the differences between control and treated cells.

The analysis of the spectra evidences the presence of signals of (i) leucine, isoleucine, valine, ethanol, lactate, pyruvate, lysine, pyroglutamate, threonine, and glucose in the spectral region from 0.0 ppm to 5.5 ppm, (ii) 1-methylhistidine, tyrosine, phenylalanine, and formate in the spectra region from 7 ppm to 8.5 ppm (Table 1; Figure 3).

**Table 1.** List of HeLa metabolic pathways affected by Crotamine uptake, using a *p*-value of Fisher's test > 5%.

| Pathway   | Coverage | Metabolites Matched | Right Tailed Fisher-Test |
|---|----------|---------------------|--------------------------|
| Transport of extracellular metabolites              | 2.13     | 13                  | $7.76 \times 10^{-11}$   |
| Protein degradation                                 | 12.73    | 7                   | $1.04 \times 10^{-10}$   |
| Aminoacyl-tRNA biosynthesis                         | 11.11    | 7                   | $2.81 \times 10^{-10}$   |
| Artificial reactions                                | 8.97     | 7                   | $1.31 \times 10^{-9}$    |
| Transport to mitochondria                           | 3.56     | 9                   | $9.39 \times 10^{-9}$    |
| Transport lysosomal                                 | 5.26     | 7                   | $5.71 \times 10^{-8}$    |
| Glycolysis/Gluconeogenesis                          | 7.81     | 5                   | $1.01 \times 10^{-6}$    |
| Transport peroxisomal                               | 3.88     | 4                   | $2.38 \times 10^{-4}$    |
| Pyruvate metabolism                                 | 6.12     | 3                   | $4.35 \times 10^{-4}$    |
| Valine, Leucine and Isoleucine metabolism           | 4.76     | 3                   | $9.13 \times 10^{-4}$    |
| Glutathione metabolism                              | 5.56     | 2                   | $5.58 \times 10^{-3}$    |
| Tyrosine metabolism                                 | 5.56     | 2                   | $5.58 \times 10^{-3}$    |
| Phenylalanine, tyrosine and tryptophan biosynthesis | 2.5      | 3                   | $5.80 \times 10^{-3}$    |
| Transport Golgi apparatus                           | 3.64     | 2                   | $1.27 \times 10^{-2}$    |
| Cysteine and methionine metabolism                  | 3.03     | 2                   | $1.80 \times 10^{-2}$    |
| Glycine, serine and threonine metabolism            | 2.3      | 2                   | $3.02 \times 10^{-2}$    |

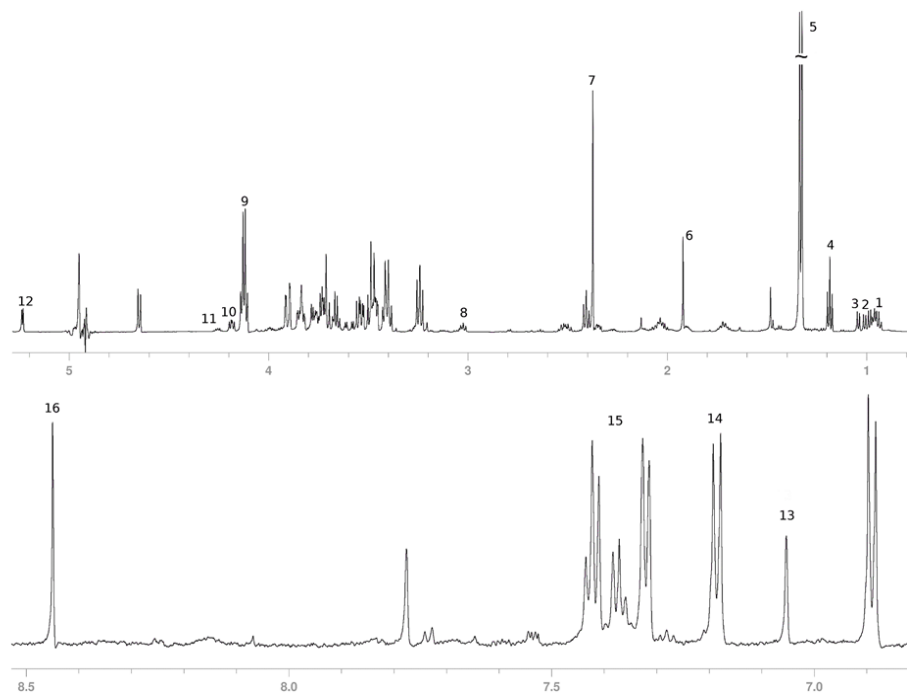


**Figure 3.** Sample NMR spectrum. NMR spectrum showing signals for: 1—Leucine; 2—Isoleucine; 3—Valine; 4—Ethanol; 5 and 9—Lactate; 6—Acetate; 7—Pyruvate; 8—Lysine; 10—Pyruglutamate; 11—Threonine; 12—Glucose; 13—1-Methylhistidine; 14—Tyrosine; 15—Phenylalanine; 16—Formate.

### 3.3. Crotamine Induced Metabolic Variation in HeLa Cells (Multivariate Data Analysis)

Multivariate data analysis was employed to analyze the changes caused by Crotamine on HeLa cells and to identify the possible metabolic pathway involved.

PCA, PLS-DA and OPLS-DA score plots show well selected controls and the treated groups in the 95% confidence interval indicate significant metabolic changes in HeLa cells as a result of the Crotamine treatment. Principal component analysis (PCA) of the  $^1\text{H}$  NMR spectra showed a clear discrimination between HeLa cell line before and after 10  $\mu\text{M}$  treatment with Crotamine (Figure 4a). To obtain information on the types of metabolites responsible for the class separation, the orthogonal projection to latent structure with discriminant analysis (OPLS-DA) was conducted with the corresponding NMR data from the cell group. As illustrated in Figure 4b, the control and Crotamine-treated groups could be clearly distinguished in the OPLS-DA score plot.

Additionally, signals that satisfy the requirements of possessing a Welch-test p-value lower than 5%, a fold change in log scale higher than 1.2 or lower than 0.8 and have high VIP score from PLS-DA loadings were selected (Figure 4c). These signals were used to metabolite identification as performed by matching chemical shifts and the scalar coupling in the Chenomx NMR software package and  $^1\text{H}$ ,  $^{13}\text{C}$ -HSQC signals. A total of 15 metabolites, presented in Figure 3 (shown in a reference NMR spectrum), Figure 5 and (Supplementary Material S1), were considered relevant for distinguishing between control and Crotamine treated cell cultures. Their levels encountered in Crotamine-treated and control samples were measured using the integral module in TopSpin 3.2 for isolated signals of each metabolite (Figure 5 and Supplementary Material S1). The measured values were scaled in MetaboAnalyst to identify which metabolic pathways are involved. The tool suggests the most relevant pathways by uploading the discriminatory compounds that were significantly influenced by Crotamine treatment. Results are displayed in Figure 5 as boxplots.

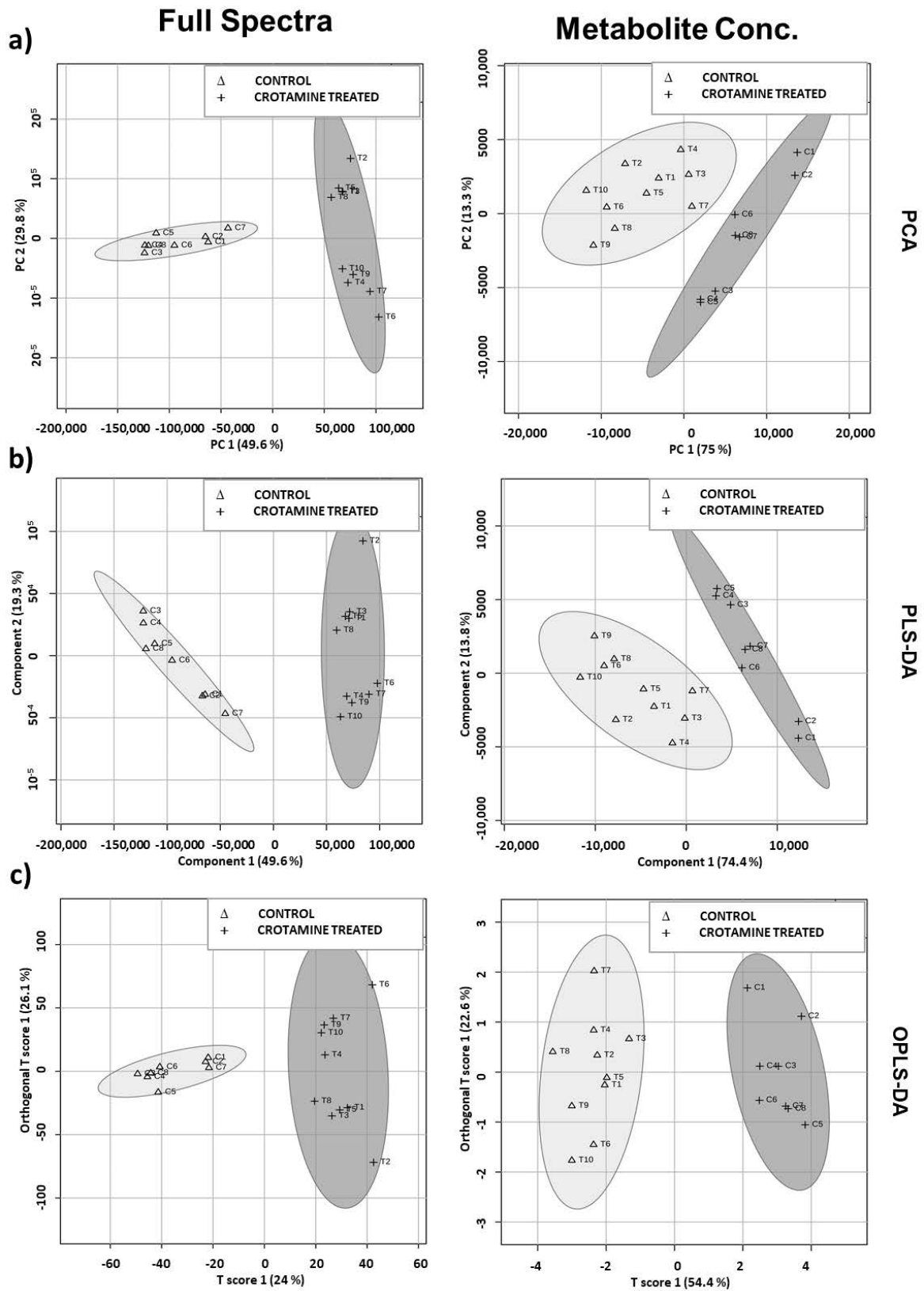


**Figure 4.** PCA (a), PLS-DA (b) and OPLS-DA (c) score plots. Principal component analysis orthogonal partial least square discriminant analysis and partial least square discriminant analysis score plots performed for full spectra bins and integral signals for selected metabolites.

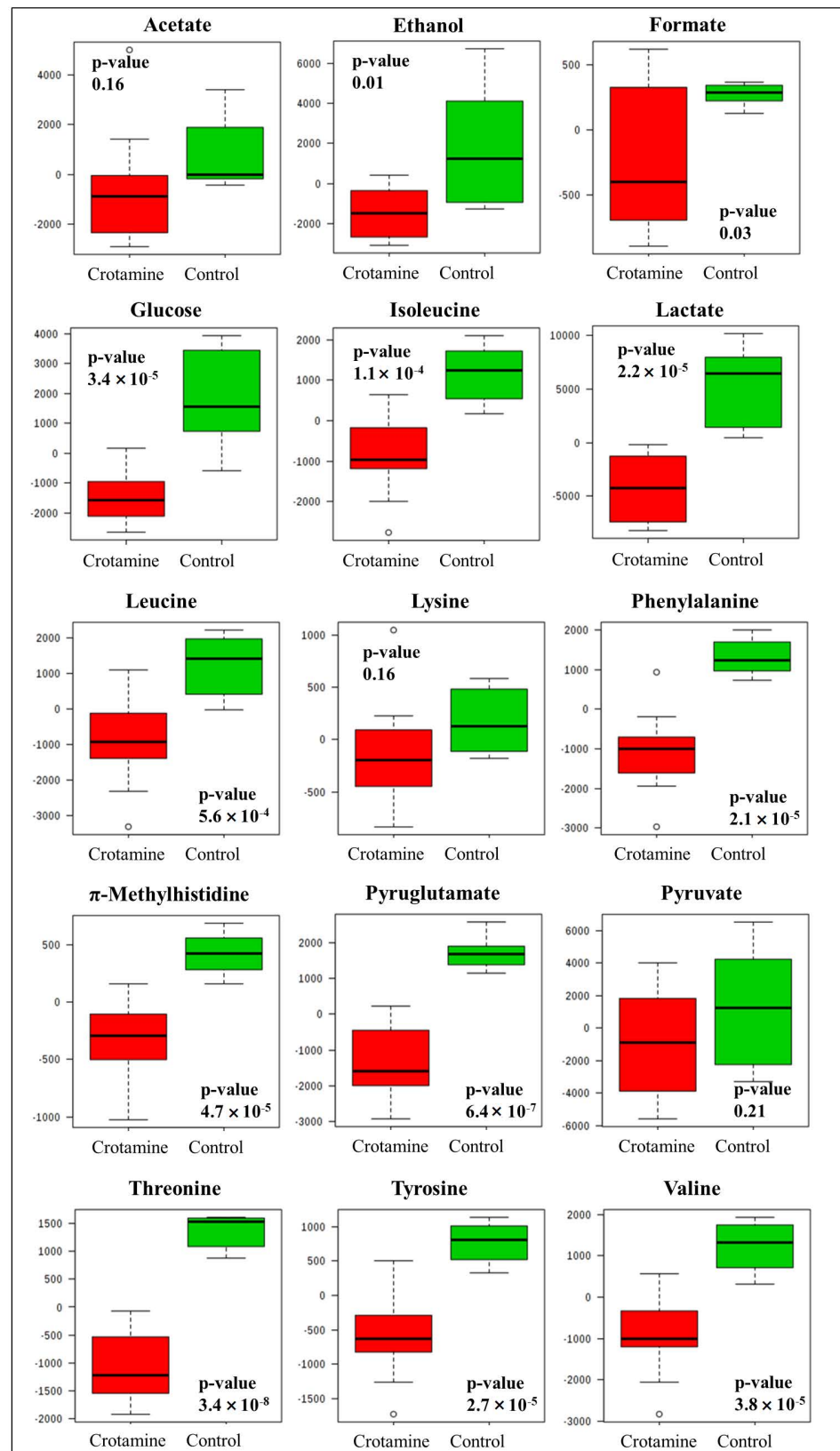


**Figure 5.** Metabolite levels in Crotonamine-treated and control samples. Distinguished metabolite levels between Crotonamine-treated and control samples. Values were evaluated from integrated isolated signals for each metabolite presented in NMR spectra and scaled in MetaboAnalyst.

In our study, the stress-related metabolic variations include the decreases of acetate, ethanol, formate, glucose, etc. The decreased levels of amino acids such as isoleucine, leucine, lysine, phenylalanine, threonine, tyrosine, and valine indicate inhibition of protein metabolism in response to Crotonamine.

Lactate and acetate release are closely correlated with the variance of the glucose utilization mainly due to cytosolic pyruvate production in glycolysis.

Each of the models developed to analyze the data provides an overview of the metabolite enrichment set as presented in Figure 6a and ranked according to metabolite importance. Classification probabilities for each sample following the Monte-Carlo cross validation is shown in Figure 6b. Perfect classification is achieved for both SVM (3 metabolite levels used) and PLS-DA (2 metabolite levels used). These results indicate that the metabolite levels used in the models can potentially be applied to differentiate between the metabolic states of control HeLa cells and following Crotonamine treatment.

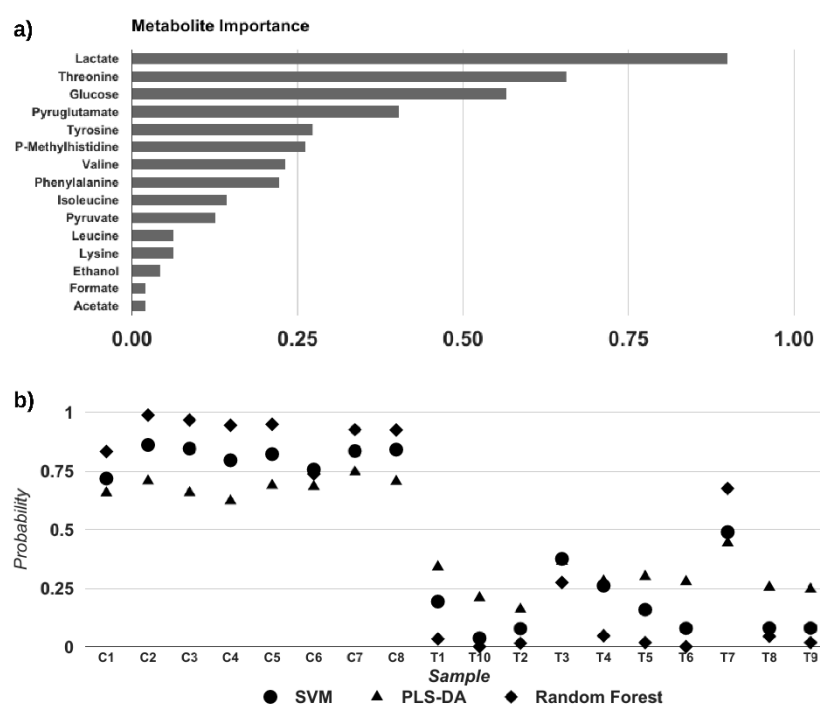


**Figure 6.** Metabolite importance measured as the average of used frequency in classification models SVM, PLS-DA and Random Forest (a). Classification probabilities for each sample tested in Monte-Carlo cross validation by classification models SVM, PLS-DA and Random Forest (b).

#### 4. Discussion

NMR is a well-known method for the identification and quantification of small organic molecules, i.e., metabolites in the sense of metabolomics. The differences in  $^1\text{H}$  resonances according to the chemical environment, lead to possible identification of hundreds of molecules in the same sample [39]. This establish NMR is a powerful tool in order to identify and quantify metabolites in different types of sample, ranging from human biofluids such as plasma/serum [40], urine [39], cerebrospinal fluid [41], plant extract [42], cell culture [43], etc.

In addition, the secreted metabolites (also referred to as secretome) are subject of studies in different levels. Senges and colleagues (2018) have identified over 1000 secreted metabolites from *Streptomyces chartreusis*. The authors show the impact of medium in the secretome, and they hypothesize that it is possible to tune a variety of metabolites to be secreted, opening an interesting gate in biotechnology. In this report, we have studied the secreted factors (secretome) from HeLa cells under influence of Crotonamine that were uploaded into the MetExplore web server and based on the metabolome analysis module,



Figure 7. Pyruvate has also shown to reduce carnosine toxicity in HeLa cells [45]. Therefore, it is possible that the reduced pyruvate concentration in crostamine treated HeLa cells could suggest a higher carnosine cytotoxicity.

Reduction in glucose levels, the third metabolite in the rank of importance, is observed in treated samples. An effect of Crostamine on the glucose and energy metabolism in animal models, using biochemical measurements of blood and urine samples, showed improved glucose tolerance and increased insulin sensitivity [29,46].

Increase in glucose uptake may be achieved by overexpressing a set of proteins known as glucose transporters [47–49], which indicate that cells are changing their metabolic state in order to increase energy production that is affected by Crostamine. Glucose can be switched on by acetate, to support the biosynthesis of fatty acids and lipids, as demonstrated in tumor-like tissue culture conditions [50–52]. One rescued acetate molecule can produce acetyl-CoA to synthesize fatty acid or sterols, to acetylation of histones, or to promote oxidation to generate additionally ~12 units of ATP, all of this process at the cost of a single ATP [53]. Some studies address the importance of acetate in cancer development [54–57]. One alternative source of carbon can be provided by acetate, as well as by glutamine if the access to the glucose-derived from acetyl-CoA is compromised by hypoxia or mitochondrial dysfunction [50,57].

Dependent on an acetyl-CoA synthetase2 (ACSS2), studies using metabolomics demonstrated that cancer-cell can capture acetate molecules to use as a carbon source [54,58]. An acetate, when ligated to CoA is the most central and dynamic metabolite in intermediary metabolism (Figure 7).

It is well documented that cancer cells generate energy differently than normal cells [54,59,60]. The process that healthy cells gain energy is very complex and requires oxygen molecules; however, the current knowledge indicates that this does not occur in cancer cells [50,61,62]. The metabolic pathway used for cancer cells to produce energy was demonstrated to be more primitive [47,50,61,62]. The less efficient process, the Warburg effect, has been studied extensively. In the 1920s, several experiments performed by Otto Warburg demonstrated that cancer cells generate energy via fermentation, similar to the process observed in yeast, even when there is a sufficient amount of oxygen available to break down glucose [63,64]. Using fermentation, which is less efficient, the cancer cells should ideally use more glucose to produce the same amount of energy, suggesting that malignant cells must rely on other sources for metabolism, like fats and amino acids [65]. Tyrosine is one of the sources that cancer prefers but is rarely used by normal healthy cells. Some in vitro studies demonstrate that the restriction in the availability of tyrosine, as also methionine, and phenylalanine affects the signaling pathway, and induces apoptosis in some cancer cells lines [66–69].

Numerous studies have shown that the restriction of specific amino acids modulates glucose consumption and the changes are closely related to glucose metabolism. In prostate cancer cells the carbohydrate metabolism is modulated by the restriction of amino acid, as shown by Fu et al., which causes modification in glucose metabolism, thereby leading to cell death and apoptosis [66,70].

Phenylalanine, one of the reduced molecules in our study, is an essential amino acid and its hydroxylation produces tyrosine. The ketogenic component, which in fact, is one important component of the tricarboxylic acid (TCA) cycle, is produced by the degradation of tyrosine to acetoacetate and fumarate (Figure 7). Oxaloacetate, which is converted from the fumarate, can be directed to the gluconeogenesis pathway. There are five amino acids entering the TCA cycle via pyruvate, these are: alanine, glycine, serine, cysteine, and tryptophan. In Crostamine-treated samples, we did not observe any changes in the level of these amino acids. However, the other amino acids that yield acetyl-CoA and/or acetoacetyl-CoA, like lysine, phenylalanine, tyrosine, leucine, and isoleucine are affected by Crostamine. On the other hand, threonine can be converted into glycine and plays a pivotal role in one-carbon metabolism and nucleotide synthesis [61]. Threonine plays a key role in cancer cell growth and proliferation [71]. Cell death and reduction in methylation

of some histone are results from the shortage of threonine in cell cultures [61,72]. There is a sequence of simultaneous events; tyrosine reduction, probably reduces the glutamate synthesis, which automatically reduces its PTM (post-translational modification), it means, the reduction of pyroglutamate, the cyclic form of glutamate.

Following the described metabolite changes, the cyclic amino acid pyroglutamate is encountered at the N-terminus of some protein and biological peptides [73], which is often involved in stabilizing the protein by making it more resistant to chemical or enzymatic degradation [74,75]. Pyroglutamate is an intermediate in glutathione metabolism, whereas glutathione (GSH) plays an important role in a multitude of cellular processes. In cancer cells, it is particularly relevant in the progression and regulation of carcinogenic mechanisms. GSH is crucial to control the reactive oxygen and its deficiency leads to a susceptibility to oxidative stress, involved in cancer progression [76]. The excess of reactive oxygen leads to cell damage as well as cancer development [77], the antioxidants often help in protecting against cancer cell formation. On the other hand, GSH is converted to a diverse compound by glutathione-S-transferase, which is responsible in regulating the pathway of mitogen-activated protein (MAP) kinase, responsible for cell survival, as well as being associated with anticancer drug resistance [78]. The probable perturbation of the GSH metabolism by Crotonamine opens the possibility of regulating the cellular response. Since, either glutamate or GSH are observed in the NMR spectra, decreased pyroglutamate levels only suggest that Crotonamine treatment alters the intracellular redox balance.

Tumor cells can reprogram metabolism in ways that support growth. Following our Crotonamine-treated HeLa cells, the BCAAs (Branched-Chain Amino Acid); leucine, isoleucine, and valine, which are essential nutrients for cancer growth, and are present in elevated concentrations impact protein synthesis and degradation [79,80]. Tumor cells utilize BCAA for protein synthesis or alternatively, oxidize them to obtain energy [81]. BCAAs are converted into their branched-chain alpha-keto acids by two aminotransferases; one present in the cytosolic space [Branched-chain aminotransferase1 (BCAT1)] and a mitochondrial [branched-chain aminotransferase2 (BCAT2)], the process occurs when the amino group is transferred to the alpha-ketoglutarate, generating glutamate [81,82], affecting the glutathione metabolism, as described earlier. The reduction level of these amino acids in Crotonamine treated cells may interfere in the BCAA degradation, and consequently in glutathione metabolism.

In the present study, the lysine concentration decreased under Crotonamine treated cells, and we presumed it was being used for cell survival and proliferation. Modifications in lysine are an important functional feature, which regulates cancer development. Dependent on acetyl-CoA, acetylation controls multiple metabolic processes and lysine acetylation is [83,84] a reversible process, which provides a functional diversity to the protein. The decreased level of lysine in HeLa-treated cells suggests that this is due to the action of Crotonamine in the acetylation process. Histidine is an amino acid that can undergo methylation. 1-methylhistidine (1-MH), a decreased metabolite in Crotonamine treated sample, is a methylated form of histidine, which is frequent in human muscles and urine. 1-methylhistidine is involved in histidine and beta-alanine metabolism [85], the latter, presented altered levels in estrogen receptor for breast cancer subtypes, as well in cancer tissue [85]. Few studies deal with the role of this metabolite in cancer cells. Indeed, 1-MH is not formed in humans and results from the metabolism of the dipeptide anserine obtained from food [86].

Formate is a metabolite produced in mammals, being a source of single-carbon group, used for purine synthesis, as well as in methylation [87,88]. Produced in different tissues from a variety of substrates, it can be synthesized during the catabolism of tryptophan. Formate production is important for a regulatory mechanism, in other words, it is important for the methylation of the DNA, RNA, and proteins [87]. The amount of formate in cancer cells seems to be two times more, compared to normal cells [87]. Meiser et al., 2018 have shown that the increase of serine catabolism to formate is associated with increased levels of circulating formate. They suggested that there is another category of cancers with putative

active oxidative metabolism that are formate overflow positive [89]. Its decrease in the presence of Crotonamine, may restrict the supply of the single-carbon group.

To conclude, acetate is related to ethanol degradation, and it is further metabolized to acetyl-CoA.

## 5. Conclusions

Following glucose uptake, cancer cell lines preferentially use glycolysis for ATP production, leading to pyruvate and lactate production. Pyruvate is directly linked to the TCA cycle and to valine, leucine and isoleucine metabolism, which in turn, is related to glutathione metabolism and to pyroglutamate levels. Glutathione is the precursor of glycine and thus, glycine, serine, and threonine metabolism are linked to the glutathione and valine, leucine and isoleucine pathways, threonine is metabolized in two ways to be converted in pyruvate. Phenylalanine is the precursor of both pyruvate and tyrosine, which in turn, may be converted to fumarate, a component of the TCA cycle. Finally, aspartate is converted to lysine, threonine and oxaloacetate, also from the TCA cycle.

It is possible to track all observed metabolites following the arrows in Figure 7, starting from glucose. Thus, the present results raise the hypothesis that Crotonamine may influence the conversion of glucose to pyruvate. Following glucose uptake, it may be consumed by glycolysis, to produce glycogen or may be used in the pentose phosphate pathway. The observation that glucose levels in the medium is reduced in Crotonamine-treated samples, indicates that its uptake is increased when compared to untreated HeLa cells. Nevertheless, both pyruvate and lactate, that are synthesized within cells and their surplus are secreted to the medium, are also found to be reduced. This suggests that Crotonamine function may be involved in impairing glycolysis. By impairing glycolysis and pyruvate production, it could also bias the TCA cycle, glutathione metabolism and amino acids biosynthesis and metabolism, as shown in Figure 7. However, due to the top-down nature of metabolomics approaches, data are inconclusive about how this could be achieved. Crotonamine is known to interact with DNA and it could be affecting specific gene expression pathways related to glycolysis or even promoting gene expression in the glycogen synthesis pathway, and in regulating glucose usage in cellular metabolism.

The exact mechanism by which Crotonamine functions as an anticancer peptide is unclear. In this metabolomics foot printing approach, the levels of certain metabolites were observed to be different following Crotonamine treatment of HeLa cells indicating that specific pathways were affected. These results provide an indication of Crotonamine function and its mechanism of action in the inhibition of cancer cell growth. Specifically, Crotonamine impairs glycolysis, and interferes with other pathways involved in glutathione metabolism, the TCA cycle and amino acid biosynthesis and metabolism.

A total of 15 metabolites were changed in the treated sample and provide potential information in cancer progression. Further investigation is needed to validate these initial findings.

**Supplementary Materials:** The following supporting information can be downloaded at: <https://www.mdpi.com/article/10.3390/biomed2020020/s1>, Material S1: NMR assignments of the identified metabolites.

**Author Contributions:** Conceptualization, M.A.C.; methodology, M.A.C. and F.R.d.M.; validation, M.A.C., F.R.d.M., R.J.E., B.S. and M.F.C.; formal analysis, M.A.C., F.R.d.M., B.S. and M.F.C.; investigation, M.A.C., F.R.d.M. and B.S.; resources, P.R. and R.K.A.; writing—original draft preparation, M.A.C., F.R.d.M. and B.S.; writing—review and editing, M.A.C., F.R.d.M., B.S., M.F.C., R.J.E., P.R. and R.K.A. All authors have read and agreed to the published version of the manuscript.

**Funding:** This research was supported by grants from CNPq [Grant numbers 435913/2016-6, 401270/2014-9, 307338/2014-2, 150444/2017-6, 309940/2019-2], FAPESP [Grant numbers 2015/13765-0, 2015/18868-2, 2016/08104-8; 2009/53989-4], CAPES and PROPe UNESP.

**Institutional Review Board Statement:** Not applicable.

**Informed Consent Statement:** Not applicable.

**Data Availability Statement:** The data that support the findings of this study are available on request from the corresponding author, [M.A.C.].

**Conflicts of Interest:** The authors declare no conflict of interest.

## References

1. Hassanpour, S.H.; Dehghani, M. Review of cancer from perspective of molecular. *J. Cancer Res. Pract.* **2017**, *4*, 127–129. [[CrossRef](#)]
2. Fitzmaurice, C.; Allen, C.; Barber, R.M.; Barregard, L.; Bhutta, Z.A.; Brenner, H.; Dicker, D.J.; Chimed-Orchir, O.; Dandona, R.; Dandona, L.; et al. Global, Regional, and National Cancer Incidence, Mortality, Years of Life Lost, Years Lived with Disability, and Disability-Adjusted Life-years for 32 Cancer Groups, 1990 to 2015: A systematic analysis for the global burden of disease study. *JAMA Oncol.* **2017**, *3*, 524–548. [[CrossRef](#)] [[PubMed](#)]
3. Lorenzi, A.T.; Syrjänen, K.J.; Longatto-Filho, A. Human papillomavirus (HPV) screening and cervical cancer burden. A Brazilian perspective. *Viol. J.* **2015**, *12*, 112. [[CrossRef](#)] [[PubMed](#)]
4. Syrjänen, K.; Syrjänen, S. *Papillomavirus Infections in Human Pathology*, 1st ed.; John Wiley & Sons: New York, NY, USA, 2000.
5. Coelho, F.R.G.F.; Fregnani, J.; Zeferino, J.H.T.G.; Villa, L.C.; Federico, L.L.; Novaes, M.H.; Costa, P.E.R.S. *Câncer do Colo do Útero*; Tecmedd: São Paulo, Brazil, 2008.
6. Ferlay, J.; Soerjomataram, I.; Dikshit, R.; Eser, S.; Mathers, C.; Rebelo, M.; Parkin, D.M.; Forman, D.; Bray, F. Cancer incidence and mortality worldwide: Sources, methods and major patterns in GLOBOCAN 2012. *Int. J. Cancer* **2015**, *136*, E359–E386. [[CrossRef](#)] [[PubMed](#)]
7. Ervik, M.; Lam, F.; Ferlay, J.; Mery, L.; Soerjomataram, I.; Bray, F. Cancer Today. Lyon, France: International Agency for Research on Cancer. Cancer Today. 2015. Available online: <http://gco.iarc.fr/today> (accessed on 22 November 2021).
8. Ferlay, J.; Colombet, M.; Soerjomataram, I.; Mathers, C.; Parkin, D.M.; Piñeros, M.; Znaor, A.; Bray, F. Estimating the global cancer incidence and mortality in 2018: GLOBOCAN sources and methods. *Int. J. Cancer* **2019**, *144*, 1941–1953. [[CrossRef](#)] [[PubMed](#)]
9. Sung, H.; Ferlay, J.; Siegel, R.L.; Laversanne, M.; Soerjomataram, I.; Jemal, A.; Bray, F. Global Cancer Statistics 2020: GLOBOCAN Estimates of Incidence and Mortality Worldwide for 36 Cancers in 185 Countries. *CA Cancer J. Clin.* **2021**, *71*, 209–249. [[CrossRef](#)] [[PubMed](#)]
10. INCA. Coordenação de Prevenção e Vigilância Brasil. Rio de Janeiro: Ministério da Saúde; Instituto Nacional de Câncer—Estimativa. 2018. Available online: <https://www.inca.gov.br/tipos-de-cancer/cancer-do-colo-do-utero> (accessed on 10 January 2019).
11. Cushman, D.W.; Ondetti, M.A. History of the design of captopril and related inhibitors of angiotensin converting enzyme. *Hypertension* **1991**, *17*, 589–592. [[CrossRef](#)]
12. Vyas, V.K.; Brahmabhatta, K.; Bhatta, H.; Parmar, U.; Patidar, R. Therapeutic potential of snake venom in cancer therapy: Current perspectives. *Asian Pac. J. Trop. Biomed.* **2013**, *3*, 156–162. [[CrossRef](#)]
13. Shanbhag, V.K.L. Applications of snake venoms in treatment of cancer. *Asian Pac. J. Trop. Biomed.* **2015**, *5*, 275–276. [[CrossRef](#)]
14. Nicastro, G.; Franzoni, L.; de Chiara, C.; Mancin, A.C.; Giglio, J.R.; Spisni, A. Solution structure of crotamine, a Na<sup>+</sup> channel affecting toxin from *Crotalus durissus terrificus* venom. *J. Biol. Inorg. Chem.* **2003**, *270*, 1969–1979. [[CrossRef](#)]
15. Fadel, V.; Bettendorff, P.; Herrmann, T.; de Azevedo, W.F., Jr.; Oliveira, E.B.; Yamane, T.; Wüthrich, K. Automated NMR structure determination and disulfide bond identification of the myotoxin crotamine from *Crotalus durissus terrificus*. *Toxicon* **2005**, *46*, 759–767. [[CrossRef](#)] [[PubMed](#)]
16. Coronado, M.A.; Gabdulkhakov, A.; Georgieva, D.; Sankaran, B.; Murakami, M.T.; Arni, R.K.; Betzel, C. Structure of the polypeptide crotamine from the Brazilian rattlesnake *Crotalus durissus terrificus*. *Acta Crystallogr. Sect. D Biol. Crystallogr.* **2013**, *69*, 1958–1964. [[CrossRef](#)]
17. Fawell, S.; Seery, J.; Daikh, Y.; Moore, C.; Chen, L.L.; Pepinsky, B.; Barsoum, J. Tat-mediated delivery of heterologous proteins into cells. *Proc. Natl. Acad. Sci. USA* **1994**, *91*, 664–668. [[CrossRef](#)]
18. Vivès, E.; Brodin, P.; Lebleu, B. A Truncated HIV-1 Tat Protein Basic Domain Rapidly Translocates through the Plasma Membrane and Accumulates in the Cell Nucleus. *J. Biol. Chem.* **1997**, *272*, 16010–16017. [[CrossRef](#)]
19. Schwarze, S.R.; Ho, A.; Vocero-Akbani, A.; Dowdy, S.F. In Vivo Protein Transduction: Delivery of a Biologically Active Protein into the Mouse. *Science* **1999**, *285*, 1569–1572. [[CrossRef](#)] [[PubMed](#)]
20. Yamane, E.S.; Bizerra, F.C.; Oliveira, E.B.; Moreira, J.T.; Rajabi, M.; Nunes, G.L.; de Souza, A.O.; da Silva, I.D.; Yamane, T.; Karpel, R.L.; et al. Unraveling the antifungal activity of a South American rattlesnake toxin crotamine. *Biochimie* **2013**, *95*, 231–240. [[CrossRef](#)] [[PubMed](#)]
21. Kerkis, I.; Hayashi, M.A.F.; Prieto da Silva, A.R.B.; Pereira, A.; De Sá Júnior, P.L.; Zaharenko, A.J.; Rádis-Baptista, G.; Kerkis, A.; Yamane, T. State of the Art in the Studies on Crotamine, a Cell Penetrating Peptide from South American Rattlesnake. *BioMed Res. Int.* **2014**, *2014*, 675985. [[CrossRef](#)] [[PubMed](#)]
22. Kerkis, A.; Kerkis, I.; Rádis-Baptista, G.; Oliveira, E.B.; Vianna-Morgante, A.M.; Pereira, L.V.; Yamane, T. Crotamine is a novel cell-penetrating protein from the venom of rattlesnake *Crotalus durissus terrificus*. *FASEB J.* **2004**, *18*, 1407–1409. [[CrossRef](#)]

23. Pereira, A.; Kerkis, A.; Hayashi, M.A.; Pereira, A.S.; Silva, F.S.; Oliveira, E.B.; Prieto da Silva, A.R.B.; Yamane, T.; Rádis-Baptista, G.; Kerkis, I. Crotonamine toxicity and efficacy in mouse models of melanoma. *Expert Opin. Investig. Drugs* **2011**, *20*, 1189–1200. [[CrossRef](#)]
24. Kerkis, A.; Hayashi, M.A.F.; Yamane, T.; Kerkis, I. Properties of cell penetrating peptides (CPPs). *IUBMB Life* **2006**, *58*, 7–13. [[CrossRef](#)]
25. Caron, N.J.; Torrente, Y.; Camirand, G.; Bujold, M.; Chapdelaine, P.; Leriche, K.; Bresolin, N.; Tremblay, J.P. Intracellular Delivery of a Tat-eGFP Fusion Protein into Muscle Cells. *Mol. Ther.* **2001**, *3*, 310–318. [[CrossRef](#)] [[PubMed](#)]
26. Derossi, D.; Chassaing, G.; Prochiantz, A. Trojan peptides: The penetratin system for intracellular delivery. *Trends Cell Biol.* **1998**, *8*, 84–87. [[CrossRef](#)]
27. Nascimento, F.D.; Hayashi, M.A.F.; Kerkis, A.; Oliveira, V.; Oliveira, E.B.; Rádis-Baptista, G.; Nader, H.B.; Yamane, T.; dos Santos Tersariol, I.L.; Kerkis, I. Crotonamine Mediates Gene Delivery into Cells through the Binding to Heparan Sulfate Proteoglycans. *J. Biol. Chem.* **2007**, *282*, 21349–21360. [[CrossRef](#)] [[PubMed](#)]
28. Harada, H.; Kizaka-Kondoh, S.; Hiraoka, M. Antitumor protein therapy; Application of the protein transduction domain to the development of a protein drug for cancer treatment. *Breast Cancer* **2006**, *13*, 16–26. [[CrossRef](#)]
29. Campeiro, J.D.; Marinovic, M.P.; Carapeto, F.C.; Mas, C.D.; Monte, G.G.; Porta, L.C.; Nering, M.B.; Oliveira, E.B.; Hayashi, M.A.F. Oral treatment with a rattlesnake native polypeptide crotonamine efficiently inhibits the tumor growth with no potential toxicity for the host animal and with suggestive positive effects on animal metabolic profile. *Amino Acids* **2017**, *50*, 267–278. [[CrossRef](#)]
30. Nascimento, F.D.; Sancey, L.; Pereira, A.; Rome, C.; Oliveira, V.; Oliveira, E.B.; Nader, H.B.; Yamane, T.; Kerkis, I.; Tersariol, I.L.S.; et al. The Natural Cell-Penetrating Peptide Crotonamine Targets Tumor Tissue in Vivo and Triggers a Lethal Calcium-Dependent Pathway in Cultured Cells. *Mol. Pharm.* **2012**, *9*, 211–221. [[CrossRef](#)]
31. Feng, J.; Zhao, J.; Hao, F.; Chen, C.; Bhakoo, K.; Tang, H. NMR-based metabolomics analyses of the effects of ultra-small super paramagnetic particles of iron oxide (USPIO) on macrophage metabolism. *J. Nanopart. Res.* **2011**, *13*, 2049–2062. [[CrossRef](#)]
32. Feng, J.; Li, J.; Wu, H.; Chen, Z. Metabolic responses of HeLa cells to silica nanoparticles by NMR-based metabolomic analyses. *Metabolomics* **2013**, *9*, 874–886. [[CrossRef](#)]
33. Oliveira, A.B.B.; De Moraes, F.R.; Candido, N.M.; Sampaio, I.; Paula, A.S.; De Vasconcellos, A.; Silva, T.C.; Miller, A.H.; Rahal, P.; Nery, J.G.; et al. Metabolic Effects of Cobalt Ferrite Nanoparticles on Cervical Carcinoma Cells and Nontumorigenic Keratinocytes. *J. Proteome Res.* **2016**, *15*, 4337–4348. [[CrossRef](#)]
34. Xia, J.; Sinelnikov, I.V.; Han, B.; Wishart, D.S. MetaboAnalyst 3.0—Making metabolomics more meaningful. *Nucleic Acids Res.* **2015**, *43*, W251–W257. [[CrossRef](#)]
35. Wishart, D.S.; Jewison, T.; Guo, A.C.; Wilson, M.; Knox, C.; Liu, Y.; Djoumbou, Y.; Mandal, R.; Aziat, F.; Dong, E.; et al. HMDB 3.0—The Human Metabolome Database in 2013. *Nucleic Acids Res.* **2013**, *41*, D801–D807. [[CrossRef](#)] [[PubMed](#)]
36. Mardinoglu, A.; Nielsen, J. Systems medicine and metabolic modelling. *J. Intern. Med.* **2012**, *271*, 142–154. [[CrossRef](#)] [[PubMed](#)]
37. Ghaffari, P.; Mardinoglu, A.; Asplund, A.; Shoaie, S.; Kampf, C.; Uhlen, M.; Nielsen, J. Identifying anti-growth factors for human cancer cell lines through genome-scale metabolic modeling. *Sci. Rep.* **2015**, *5*, 08183. [[CrossRef](#)] [[PubMed](#)]
38. Cottret, L.; Wildridge, D.; Vinson, F.; Barrett, M.; Charles, H.; Sagot, M.-F.; Jourdan, F. MetExplore: A web server to link metabolomic experiments and genome-scale metabolic networks. *Nucleic Acids Res.* **2010**, *38*, W132–W137. [[CrossRef](#)] [[PubMed](#)]
39. Bouatra, S.; Aziat, F.; Mandal, R.; Guo, A.C.; Wilson, M.R.; Knox, C.; Bjorn Dahl, T.C.; Krishnamurthy, R.; Saleem, F.; Liu, P.; et al. The Human Urine Metabolome. *PLoS ONE* **2013**, *8*, e73076. [[CrossRef](#)]
40. Psychogios, N.; Hau, D.D.; Peng, J.; Guo, A.C.; Mandal, R.; Bouatra, S.; Sinelnikov, I.; Krishnamurthy, R.; Eisner, R.; Gautam, B.; et al. The Human Serum Metabolome. *PLoS ONE* **2011**, *6*, e16957. [[CrossRef](#)]
41. Wishart, D.S.; Lewis, M.J.; Morrissey, J.A.; Flegel, M.D.; Jerončić, K.; Xiong, Y.; Cheng, D.; Eisner, R.; Gautam, B.; Tzur, D.; et al. The human cerebrospinal fluid metabolome. *J. Chromatogr. B* **2008**, *871*, 164–173. [[CrossRef](#)]
42. Selegato, D.M.; Pilon, A.C.; Neto, F.C. Plant Metabolomics Using NMR Spectroscopy. *Methods Pharmacol. Toxicol.* **2019**, *2037*, 345–362. [[CrossRef](#)]
43. Čuperlović-Culf, M.; Barnett, D.A.; Culf, A.S.; Chute, I. Cell culture metabolomics: Applications and future directions. *Drug Discov. Today* **2010**, *15*, 610–621. [[CrossRef](#)]
44. Chen, X.-S.; Li, L.-Y.; Guan, Y.-D.; Yang, J.-M.; Cheng, Y. Anticancer strategies based on the metabolic profile of tumor cells: Therapeutic targeting of the Warburg effect. *Acta Pharmacol. Sin.* **2016**, *37*, 1013–1019. [[CrossRef](#)]
45. Holliday, R.; McFarland, G.A. Inhibition of the growth of transformed and neoplastic cells by the dipeptide carnosine. *Br. J. Cancer* **1996**, *73*, 966–971. [[CrossRef](#)] [[PubMed](#)]
46. Marinovic, M.P.; Campeiro, J.D.; Lima, S.C.; Rocha, A.L.; Nering, M.B.; Oliveira, E.B.; Mori, M.A.; Hayashi, M.A.F. Crotonamine induces browning of adipose tissue and increases energy expenditure in mice. *Sci. Rep.* **2018**, *8*, 1–12. [[CrossRef](#)] [[PubMed](#)]
47. Schug, Z.T.; Peck, B.; Jones, D.T.; Zhang, Q.; Grosskurth, S.; Alam, I.S.; Goodwin, L.M.; Smethurst, E.; Mason, S.; Blyth, K.; et al. Acetyl-CoA Synthetase 2 Promotes Acetate Utilization and Maintains Cancer Cell Growth under Metabolic Stress. *Cancer Cell* **2015**, *27*, 57–71. [[CrossRef](#)] [[PubMed](#)]
48. Adekola, K.; Rosen, S.T.; Shanmugam, M. Glucose transporters in cancer metabolism. *Curr. Opin. Oncol.* **2012**, *24*, 650–654. [[CrossRef](#)]
49. Jóźwiak, P.; Krześlak, A.; Bryś, M.; Lipińska, A. Glucose-dependent glucose transporter 1 expression and its impact on viability of thyroid cancer cells. *Oncol. Rep.* **2014**, *33*, 913–920. [[CrossRef](#)]

50. Labak, C.M.; Wang, P.Y.; Arora, R.; Guda, M.; Asuthkar, S.; Tsung, A.J.; Velpula, K.K. Glucose transport: Meeting the meta-bolic demands of cancer, and applications in glioblastoma treatment. *Am. J. Cancer Res.* **2016**, *6*, 1599–1608.
51. Zhao, S.; Torres, A.; Henry, R.A.; Trefely, S.; Wallace, M.; Lee, J.V.; Carrer, A.; Sengupta, A.; Campbell, S.L.; Kuo, Y.-M.; et al. ATP-Citrate Lyase Controls a Glucose-to-Acetate Metabolic Switch. *Cell Rep.* **2016**, *17*, 1037–1052. [[CrossRef](#)]
52. Lakhter, A.J.; Hamilton, J.; Konger, R.L.; Brustovetsky, N.; Broxmeyer, H.E.; Naidu, S.R. Glucose-independent Acetate Metabolism Promotes Melanoma Cell Survival and Tumor Growth. *J. Biol. Chem.* **2016**, *291*, 21869–21879. [[CrossRef](#)]
53. Comerford, S.A.; Huang, Z.; Du, X.; Wang, Y.; Cai, L.; Witkiewicz, A.K.; Walters, H.; Tantawy, M.N.; Fu, A.; Manning, H.C.; et al. Acetate Dependence of Tumors. *Cell* **2014**, *159*, 1591–1602. [[CrossRef](#)]
54. Yoshii, Y.; Furukawa, T.; Yoshii, H.; Mori, T.; Kiyono, Y.; Waki, A.; Kobayashi, M.; Tsujikawa, T.; Kudo, T.; Okazawa, H.; et al. Cytosolic acetyl-CoA synthetase affected tumor cell survival under hypoxia: The possible function in tumor acetyl-CoA/acetate metabolism. *Cancer Sci.* **2009**, *100*, 821–827. [[CrossRef](#)]
55. Yoshii, Y.; Waki, A.; Furukawa, T.; Kiyono, Y.; Mori, T.; Yoshii, H.; Kudo, T.; Okazawa, H.; Welch, M.J.; Fujibayashi, Y. Tumor uptake of radiolabeled acetate reflects the expression of cytosolic acetyl-CoA synthetase: Implications for the mechanism of acetate PET. *Nucl. Med. Biol.* **2009**, *36*, 771–777. [[CrossRef](#)] [[PubMed](#)]
56. Mashimo, T.; Pichumani, K.; Vemireddy, V.; Hatanpaa, K.J.; Singh, D.K.; Sirasanagandla, S.; Nannepaga, S.; Piccirillo, S.G.M.; Kovacs, Z.; Foong, C.; et al. Acetate Is a Bioenergetic Substrate for Human Glioblastoma and Brain Metastases. *Cell* **2014**, *159*, 1603–1614. [[CrossRef](#)] [[PubMed](#)]
57. Yang, C.; Ko, B.; Hensley, C.T.; Jiang, L.; Wasti, A.T.; Kim, J.; Sudderth, J.; Calvaruso, M.A.; Lumata, L.; Mitsche, M.; et al. Glutamine Oxidation Maintains the TCA Cycle and Cell Survival during Impaired Mitochondrial Pyruvate Transport. *Mol. Cell* **2014**, *56*, 414–424. [[CrossRef](#)] [[PubMed](#)]
58. Ghaffari, P.; Mardinoglu, A.; Nielsen, J. Cancer Metabolism: A Modeling Perspective. *Front. Physiol.* **2015**, *6*, 382. [[CrossRef](#)] [[PubMed](#)]
59. Epstein, T.; Gatenby, R.A.; Brown, J.S. The Warburg effect as an adaptation of cancer cells to rapid fluctuations in energy demand. *PLoS ONE* **2017**, *12*, e0185085. [[CrossRef](#)]
60. Kim, S.-Y. Cancer Energy Metabolism: Shutting Power off Cancer Factory. *Biomol. Ther.* **2018**, *26*, 39–44. [[CrossRef](#)]
61. Amelio, I.; Cutruzzolá, F.; Antonov, A.; Agostini, M.; Melino, G. Serine and glycine metabolism in cancer. *Trends Biochem. Sci.* **2014**, *39*, 191–198. [[CrossRef](#)]
62. Fadaka, A.; Ajiboye, B.; Ojo, O.; Adewale, O.; Olayide, I.; Emuowhochere, R. Biology of glucose metabolism in cancer cells. *J. Oncol. Sci.* **2017**, *3*, 45–51. [[CrossRef](#)]
63. Warburg, O.; Wind, F.; Negelein, E. The metabolism of tumors in the body. *J. Gen. Physiol.* **1927**, *8*, 519–530. [[CrossRef](#)]
64. Liberti, M.V.; Locasale, J.W. The Warburg Effect: How Does it Benefit Cancer Cells? *Trends Biochem. Sci.* **2016**, *41*, 211–218. [[CrossRef](#)]
65. Fu, Y.-M.; Yu, Z.-X.; Lin, H.; Fu, X.; Meadows, G.G. Selective amino acid restriction differentially affects the motility and directionality of DU145 and PC3 prostate cancer cells. *J. Cell. Physiol.* **2008**, *217*, 184–193. [[CrossRef](#)] [[PubMed](#)]
66. Kulcsár, G.; Gaál, D.; Kulcsár, P.I.; Schulcz, Á.; Czompolý, T. A mixture of amino acids and other small molecules present in the serum suppresses the growth of murine and human tumors in vivo. *Int. J. Cancer* **2012**, *132*, 1213–1221. [[CrossRef](#)] [[PubMed](#)]
67. Bonfili, L.; Cecarini, V.; Cuccioloni, M.; Angeletti, M.; Flati, V.; Corsetti, G.; Pasini, E.; Dioguardi, F.S.; Eleuteri, A.M. Essential amino acid mixtures drive cancer cells to apoptosis through proteasome inhibition and autophagy activation. *FEBS J.* **2017**, *284*, 1726–1737. [[CrossRef](#)]
68. Fu, Y.-M.; Lin, H.; Liu, X.; Fang, W.; Meadows, G.G. Cell death of prostate cancer cells by specific amino acid restriction depends on alterations of glucose metabolism. *J. Cell. Physiol.* **2010**, *224*, 491–500. [[CrossRef](#)] [[PubMed](#)]
69. Shyh-Chang, N.; Locasale, J.W.; Lyssiotis, C.A.; Zheng, Y.; Teo, R.Y.; Ratanasirintra-woot, S.; Zhang, J.; Onder, T.; Unternaehrer, J.J.; Zhu, H.; et al. Influence of Threonine Metabolism on Sadenosylmethionine and Histone Methylation. *Science* **2013**, *339*, 222–226. [[CrossRef](#)] [[PubMed](#)]
70. Krall, A.S.; Xu, S.; Graeber, T.G.; Braas, D.; Christofk, H.R. Asparagine promotes cancer cell proliferation through use as an amino acid exchange factor. *Nat. Commun.* **2016**, *7*, 11457. [[CrossRef](#)]
71. Blomback, B. *Methods in Enzymology*; Hirs, C., Ed.; Academic Press: New York, NY, USA, 1967; Volume 11, pp. 389–411.
72. Liu, Y.D.; Goetze, A.M.; Bass, R.B.; Flynn, G.C. N-terminal Glutamate to Pyroglutamate Conversion in Vivo for Human IgG2 Antibodies. *J. Biol. Chem.* **2011**, *286*, 11211–11217. [[CrossRef](#)]
73. Rink, R.; Arkema-Meter, A.; Baudoin, I.; Post, E.; Kuipers, A.; Nelemans, S.; Akanbi, M.H.J.; Moll, G. To protect peptide pharmaceuticals against peptidases. *J. Pharmacol. Toxicol. Methods* **2010**, *61*, 210–218. [[CrossRef](#)]
74. Traverso, N.; Ricciarelli, R.; Nitti, M.; Marengo, B.; Furfaro, A.L.; Pronzato, M.A.; Marinari, U.M.; Domenicotti, C. Role of Glutathione in Cancer Progression and Chemoresistance. *Oxidative Med. Cell. Longev.* **2013**, *2013*, 1–10. [[CrossRef](#)]
75. Hussain, S.P.; Hofseth, L.J.; Harris, C.C. Radical causes of cancer. *Nat. Cancer* **2003**, *3*, 276–285. [[CrossRef](#)]
76. Townsend, D.M.; Tew, K.D. The role of glutathione-S-transferase in anti-cancer drug resistance. *Oncogene* **2003**, *22*, 7369–7375. [[CrossRef](#)] [[PubMed](#)]
77. Katagiri, R.; Goto, A.; Nakagawa, T.; Nishiumi, S.; Kobayashi, T.; Hidaka, A.; Budhathoki, S.; Yamaji, T.; Sawada, N.; Shimazu, T.; et al. Increased Levels of Branched-Chain Amino Acid Associated with Increased Risk of Pancreatic Cancer in a Prospective Case-Control Study of a Large Cohort. *Gastroenterology* **2018**, *155*, 1474–1482.e1. [[CrossRef](#)] [[PubMed](#)]

78. Neinast, M.; Murashige, D.; Arany, Z. Branched Chain Amino Acids. *Annu. Rev. Physiol.* **2019**, *81*, 139–164. [[CrossRef](#)] [[PubMed](#)]
79. Ananieva, E.A.; Wilkinson, A.C. Branched-chain amino acid metabolism in cancer. *Curr. Opin. Clin. Nutr. Metab. Care* **2018**, *21*, 64–70. [[CrossRef](#)]
80. Selwan, E.M.; Edinger, A.L. Branched chain amino acid metabolism and cancer: The importance of keeping things in context. *Transl. Cancer Res.* **2017**, *6*, S578–S584. [[CrossRef](#)]
81. Zhao, S.; Xu, W.; Jiang, W.; Yu, W.; Lin, Y.; Zhang, T.; Yao, J.; Zhou, L.; Zeng, Y.; Li, H.; et al. Regulation of Cellular Metabolism by Protein Lysine Acetylation. *Science* **2010**, *327*, 1000–1004. [[CrossRef](#)]
82. Baeza, J.; Smallegan, M.J.; Denu, J.M. Mechanisms and Dynamics of Protein Acetylation in Mitochondria. *Trends Biochem. Sci.* **2016**, *41*, 231–244. [[CrossRef](#)]
83. Budczies, J.; Brockmüller, S.F.; Müller, B.M.; Barupal, D.K.; Richter-Ehrenstein, C.; Kleine-Tebbe, A.; Griffin, J.L.; Orešič, M.; Dietel, M.; Denkert, C.; et al. Comparative metabolomics of estrogen receptor positive and estrogen receptor negative breast cancer: Alterations in glutamine and beta-alanine metabolism. *J. Proteom.* **2013**, *94*, 279–288. [[CrossRef](#)]
84. Brosnan, M.E.; Brosnan, J.T. Formate: The Neglected Member of One-Carbon Metabolism. *Annu. Rev. Nutr.* **2016**, *36*, 369–388. [[CrossRef](#)]
85. Wang, H.; Wang, L.; Zhang, H.; Deng, P.; Chen, J.; Zhou, B.; Hu, J.; Zou, J.; Lu, W.; Xiang, P.; et al. <sup>1</sup>H NMR-based metabolic profiling of human rectal cancer tissue. *Mol. Cancer* **2013**, *12*, 121. [[CrossRef](#)]
86. Holeček, M. Histidine in Health and Disease: Metabolism, Physiological Importance, and Use as a Supplement. *Nutrients* **2020**, *12*, 848. [[CrossRef](#)] [[PubMed](#)]
87. Wang, L.; Chen, J.; Chen, L.; Deng, P.; Bu, Q.; Xiang, P.; Li, M.; Lu, W.; Xu, Y.; Lin, H.; et al. 1H-NMR based metabonomic profiling of human esophageal cancer tissue. *Mol. Cancer* **2013**, *12*, 25. [[CrossRef](#)] [[PubMed](#)]
88. Oizel, K.; Tait-Mulder, J.; Fernandez-De-Cossio-Diaz, J.; Pietzke, M.; Brunton, H.; Lilla, S.; Dhayade, S.; Athineos, D.; Blanco, G.R.; Sumpton, D.; et al. Formate induces a metabolic switch in nucleotide and energy metabolism. *Cell Death Dis.* **2020**, *11*, 1–14. [[CrossRef](#)] [[PubMed](#)]
89. Meiser, J.; Schuster, A.; Pietzke, M.; Voorde, J.V.; Athineos, D.; Oizel, K.; Burgos-Barragan, G.; Wit, N.; Dhayade, S.; Morton, J.; et al. Increased formate overflow is a hallmark of oxidative cancer. *Nat. Commun.* **2018**, *9*, 1–12. [[CrossRef](#)]